

Article

Experimental and Numerical Study on the Thermal Response of the Lightweight Aggregate Concrete Panels Integrated with MPCM

Lin Zhu ^{1,2,3}, Qiaoyu Wang ^{1,2,3} , Guochen Sang ^{1,2,3,*}, Zhengzheng Cao ^{4,*} and Yi Xue ^{1,2,3}

- ¹ State Key Laboratory of Eco-Hydraulics in Northwest Arid Region, Xi'an University of Technology, Xi'an 710048, China; zl@xaut.edu.cn (L.Z.); 2210720052@stu.xaut.edu.cn (Q.W.); xueyi@xaut.edu.cn (Y.X.)
- ² School of Civil Engineering and Architecture, Xi'an University of Technology, Xi'an 710048, China
- ³ Shaanxi Key Laboratory of Loess Mechanics and Engineering, Xi'an University of Technology, Xi'an 710048, China
- ⁴ International Joint Research Laboratory of Henan Province for Underground Space Development and Disaster Prevention, Henan Polytechnic University, Jiaozuo 454099, China
- * Correspondence: sangguochen@xaut.edu.cn (G.S.); caozz@hpu.edu.cn (Z.C.)

Abstract: This paper determines the best design parameters and uses conditions of lightweight aggregate concrete panels containing microencapsulated phase change materials (MPCM-LWAC panels). The main work of this paper includes the followings: (1) The fundamental properties (dry density, thermal conductivity, and specific heat capacity) of MPCM-LWAC were researched to reveal the effect of MPCM dosage on these properties. (2) A model test was carried out to quantify the effect of MPCM dosage on the thermal response of the MPCM-LWAC panel exposed to realistic climate conditions. (3) The numerical simulation was conducted to investigate the effect of MPCM dosage, panel thickness, and outdoor temperature conditions on the thermal response of the MPCM-LWAC panel, which helps to determine its optimum design parameters and use condition. The results showed that the incorporation of MPCM results in lower dry density and thermal conductivity of MPCM-LWAC but higher specific heat capacity. The more MPCM dosage in the MPCM-LWAC panel with a thickness of 35 mm, the lower the energy demand to keep a comfortable interior temperature. Most notably, when the panel thickness exceeds 105 mm, the MPCM-LWAC panel with 5% MPCM only delays the peak temperature. Moreover, the optimal use condition for MPCM-LWAC panels is an average outdoor temperature of 25 °C, which makes the energy demand attain a minimum.

Keywords: lightweight aggregate concrete; microencapsulated phase change material; thermal response; energy demand



Citation: Zhu, L.; Wang, Q.; Sang, G.; Cao, Z.; Xue, Y. Experimental and Numerical Study on the Thermal Response of the Lightweight Aggregate Concrete Panels Integrated with MPCM. *Buildings* **2024**, *14*, 234. <https://doi.org/10.3390/buildings14010234>

Academic Editor: Md Morshed Alam

Received: 6 December 2023

Revised: 2 January 2024

Accepted: 11 January 2024

Published: 15 January 2024



Copyright: © 2024 by the authors. Licensee MDPI, Basel, Switzerland. This article is an open access article distributed under the terms and conditions of the Creative Commons Attribution (CC BY) license (<https://creativecommons.org/licenses/by/4.0/>).

1. Introduction

A 2022 Research Report on China's Building Energy Consumption and Carbon Emissions shows that our country's total energy consumption nationwide has reached 45% of the total energy, and building energy consumption (energy consumed by heating, cooling, ventilation, hot water, lighting, household appliances, and cooking and other supplies) accounts for 21.3% of the total energy [1]. Among them, the energy consumption used for heating and cooling is upwards of 70% of building energy consumption [2–5]. The thermal performance of the building envelope plays a critical role in energy consumption for heating and cooling [6,7]. Hence, the measures to improve the thermal performance of building envelopes are imperative.

Abundant work has shown that adding the phase change materials (PCM) into concrete can improve the thermal inertia of concrete materials without increasing the energy consumption [8,9], which is due to the advantages of PCM with high energy storage density, absorbing or releasing energy in small temperature intervals, and the phase transition

without accompanying volume change [10–12]. Much recent research has been conducted to investigate the properties of PCM concrete [13–16].

Zhu et al. [17] used the phase change ceramsite as coarse aggregate to prepare thermal storage concrete for investigating its thermal performance. This study found that thermal storage concrete can reduce indoor temperature fluctuations. Memon et al. [18] prepared the concrete with thermoregulatory properties by adding the porous lightweight aggregate adsorbed with PCM. They found that the energy storage concrete can flatten the indoor temperature fluctuations and keep the load away from peak hours. In the case of large day and night temperature differences, the thermoregulatory properties were further improved. Li et al. [19] carried out an experiment to investigate the thermal response of concrete with PCM, and the study showed that PCM concrete can effectively reduce the peak temperature and delay the appearance time of peak temperature. The temperature regulation ability of PCM concrete was directly proportional to the admixture of PCM. Urgessa et al. [20] first fabricated MPCM by using melamine formaldehyde resin to encapsulate PCM with low transition temperature. Then, the thermal storage concrete was prepared by adding the fabricated MPCM into the concrete mixture to investigate the thermal response of MPCM concrete slabs exposed to real climatic environments. Their findings showed that temperature fluctuations indoors were reduced when the ambient temperature was near the phase change temperature. Yin et al. [21] prepared the thermal storage foam concrete with PCM and investigated its thermal performance. The results showed that when the PCM additive is 15%, the time for the internal surface temperature of PCM foam concrete wall to reach the highest and lowest values were extended by 1.83 h and 1.16 h, respectively. Compared with the pure foam concrete wall, the best effect was achieved when the PCM foam concrete was placed on the inside of the wall.

Lightweight aggregate concrete (LWAC) with a low self-weight and low thermal conductivity was used to prepare the thermal storage concrete by adding MPCM, which helps to develop the building structures by optimizing thermal insulation, energy storage and energy conservation [22]. However, there has been relatively little literature to study how to fully utilize the latent heat stored in concrete in practical applications. Considering the fact that the content of MPCM determines the energy storage density of MPCM-LWAC panels, the thickness affects the heat transfer process, and the outdoor temperature conditions directly determine that of the phase transition behavior, this research will study the effect of three influencing factors mentioned above on the thermal response of MPCM-LWAC panels, which contributes to yield the best design parameters and usage conditions for MPCM-LWAC panels. In this research, non-load-bearing MPCM-LWAC panels with different MPCM dosages were prepared. The effects of MPCM dosage on the dry density, thermal conductivity, and specific heat capacity of MPCM-LWAC were first investigated by performing a series of experiments. Then, the influence of MPCM dosage, thickness, and outdoor temperature conditions on the thermal response of MPCM-LWAC panels was researched by using MATLAB R2022b. Based on this, the energy demand was calculated to assess the energy-saving potential of MPCM-LWAC panels.

2. Test Materials and Methods

2.1. Raw Materials

The MPCM used in this study was purchased from Hebei Ruosen Technology Co., Ltd. It consists of an octadecane core and methyl methacrylate shell. The core/shell ratio, density, and size of MPCM are 6:4, $0.88 \text{ g}\cdot\text{cm}^{-3}$, and 1–3 μm . The experimental results obtained from the differential scanning calorimetry (DSC) test are shown in Figure 1a. From Figure 1a, it can be found that the latent heat of MPCM is 199.86 J/g for the endothermic cycle, and 169.33 J/g for the exothermic cycle. Based on the DSC curve (Figure 1a), we calculated the specific heat capacity of MPCM, as shown in Figure 1b.

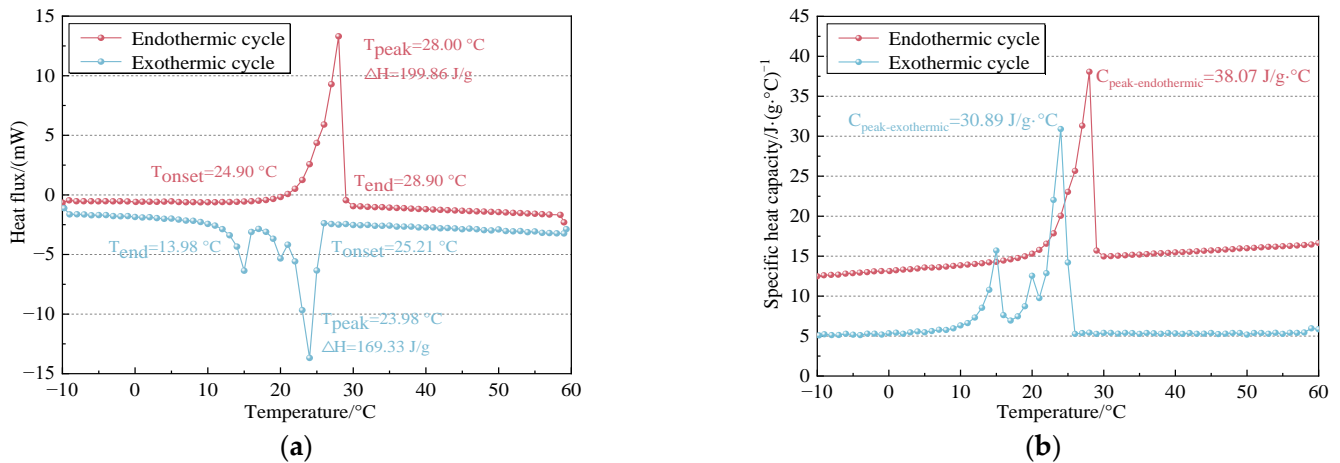


Figure 1. Phase change characteristics of MPCM: (a) DSC curve; (b) specific heat capacity.

The ceramsite with different particle sizes was selected as the lightweight coarse aggregate (LWCA) and lightweight fine aggregate (LWFA). Their basic properties were tested and shown in Figure 2.

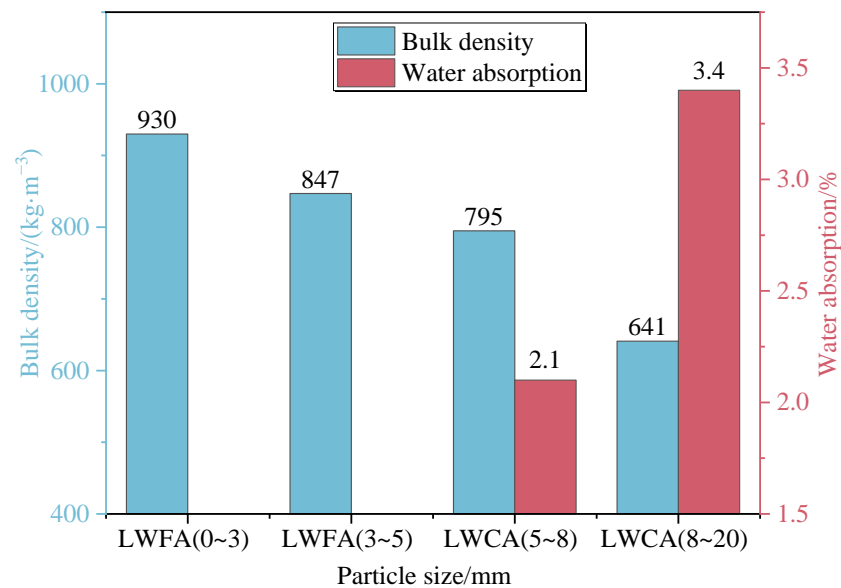


Figure 2. Properties of lightweight aggregate.

In addition, P·O42.5 ordinary Portland cement was purchased.

2.2. Mixing Proportion

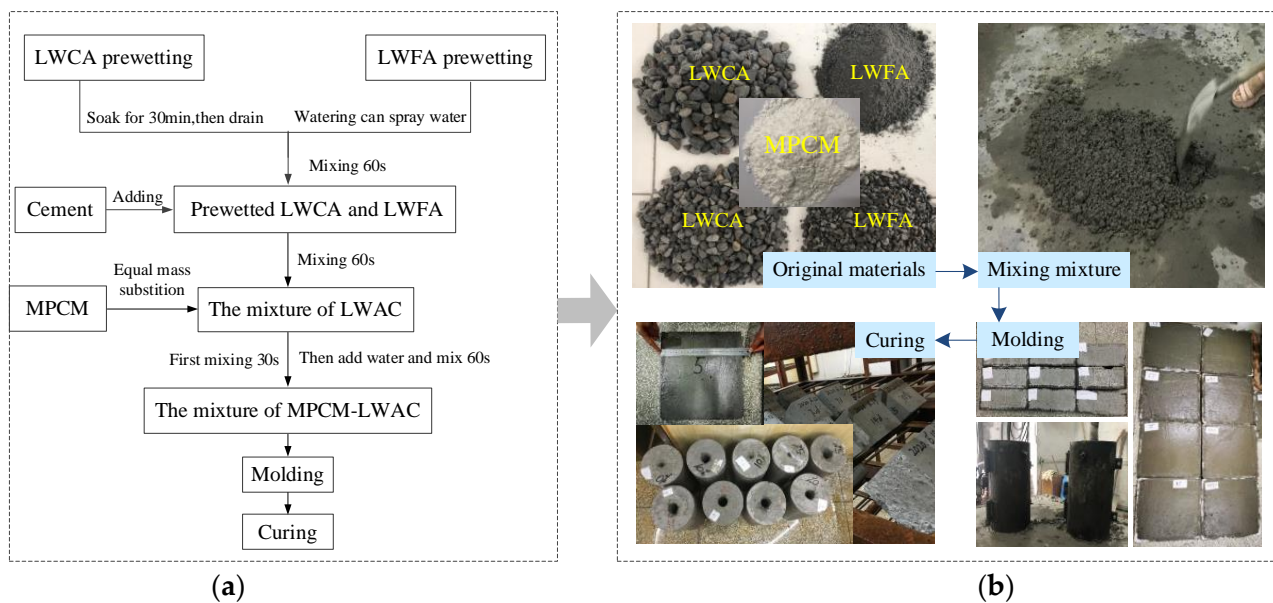
The proportion of MPCM-LWAC is given in Table 1. In this research, the method of equal mass replacement LWFA with MPCM was used to prepare the MPCM-LWAC specimens. In addition, the content of MPCM (not exceeding 10%) has been intensely studied in the preliminary study. For details, see ref. [23]. The specimen named MPCM-LWAC-0.0% in Table 1 was the LWAC without MPCM, which served as the reference group. The specimen named MPCM-LWAC-2.5% indicated that the MPCM dosage is 2.5%. The meanings of the other specimen names are followed by analogy.

Table 1. The proportion of MPCM-LWAC (kg/m³).

Sample	Water	Cement	LWCA	LWAF	MPCM
MPCM-LWAC-0.0%	187	311.7	455.5	845.80	0
MPCM-LWAC-2.5%	187	311.7	455.5	824.66	21.15
MPCM-LWAC-5.0%	187	311.7	455.5	803.51	42.29
MPCM-LWAC-7.5%	187	311.7	455.5	782.37	63.44
MPCM-LWAC-10.0%	187	311.7	455.5	761.22	84.58

2.3. Specimen Preparation

Figure 3a,b provide the preparation process and preparation overview of the MPCM-LWAC specimen, respectively. For this research, three groups of specimens were prepared. The first group was cubic specimens with a side of length 100 mm, the second group was cylindrical specimens with dimensions of $\Phi 200 \times 400$ mm², and the third group was the panel with a dimension of 300 mm \times 300 mm \times 35 mm. These three groups of specimens were used to determine the dry density, thermal conductivity, and thermal response, respectively.

**Figure 3.** Preparing MPCM-LWAC samples: (a) preparation process; (b) preparation overview.

2.4. Test Methods

Dry density: The dry density of the selected specimen was calculated by Equation (1).

$$\rho = \frac{m_d}{V} \quad (1)$$

where " ρ ", " m_d ", and " V " are the dry density, drying mass, and volume of MPCM-LWAC, respectively.

Thermal conductivity: Thermal conductivity of prepared cylindrical specimens was tested by a concrete thermophysical parameter tester (Figure 4a). Significantly, the hole with a diameter of 40 mm passing through the specimen must be set in the specimen's center. Before the experiment, sealing rings were placed on the upper and lower ends of the specimen to ensure that heat only flowed radially. Furthermore, the water and thermometer were added and arranged in the set hole and outer cavity of the specimen, as shown in Figure 4b. The specimen was first heated up to 60 °C at the beginning of the test. Then, the temperature was kept constant until the specimen reached thermal equilibrium, after which the inner and outer temperatures of the specimen and the heat flow passing through the

specimen were recorded every 10 min. Finally, the thermal conductivity for the specimen was calculated according to Equation (2).

$$\lambda = \frac{QIn\frac{r_2^2}{r_1}}{2\pi L(T_2 - T_1)} \quad (2)$$

where “ Q ” is the heat transfer from the center of the specimen to the peripheral area in the unit time, KJ/h; “ r_1 ”, “ r_2 ”, and “ L ” are inner aperture, diameter, and specimen height respectively, m; “ T_1 ” and “ T_2 ” are the temperature at the center of the specimen and the temperature of the cooling water respectively, °C.

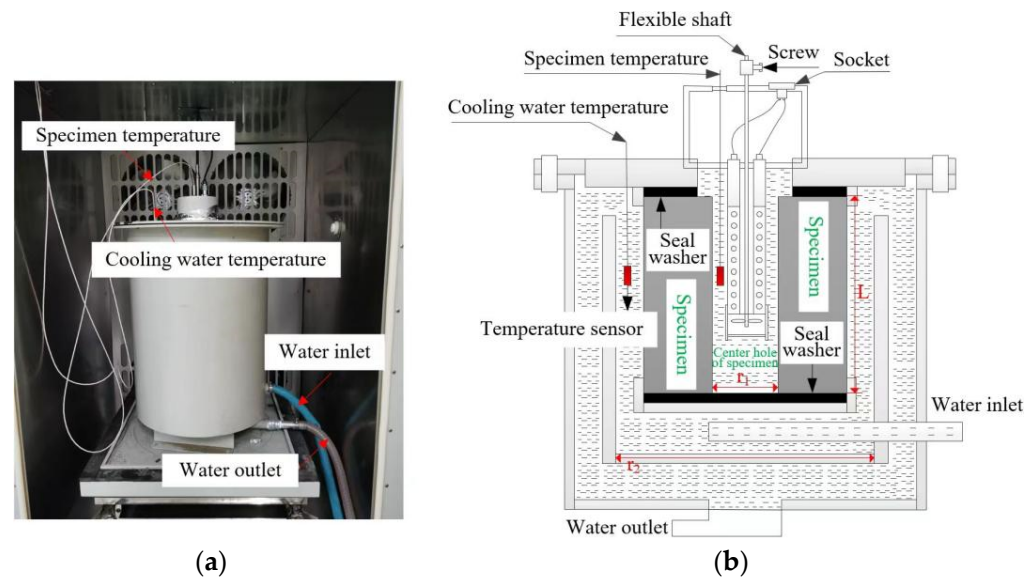


Figure 4. Thermal conductivity test: (a) concrete thermophysical parameter tester; (b) schematic diagram of tester.

Specific heat capacity: According to Equation (3), we calculated the specific heat capacity. Parameters in Equation (3) can be acquired from the DSC curves of the empty crucible (as baseline), sapphire, and MPCM-LWAC.

$$C_p = \overline{C_p} \cdot \frac{\overline{m}}{m} \cdot \frac{y}{\overline{y}} \quad (3)$$

where “ C_p ” and “ $\overline{C_p}$ ” are the specific heat capacity of MPCM-LWAC sample and sapphire, J/g·°C; “ y ” and “ \overline{y} ” are the distance difference between MPCM-LWAC sample and sapphire in the vertical coordinate; “ m ” and “ \overline{m} ” are the masses of MPCM-LWAC sample and sapphire, mg.

Thermal response: A model box with inner dimensions of $300 \times 300 \times 300 \text{ mm}^3$ was made to investigate the thermal response. To prevent heat transfer around the model box, the five-sided model box was insulated with a 40 mm rubber and plastic plate. The panels with a size of $300 \times 300 \times 35 \text{ mm}^3$ were inserted into the top of the box. The sensors of heat flow and temperature were arranged on the inside and outside surfaces of the tested panel for recording the heat flow and temperature. The model boxes were placed in a real climate environment (summer in Xi’an) for 14 days (15–29 June) for real-time testing (Figure 5).

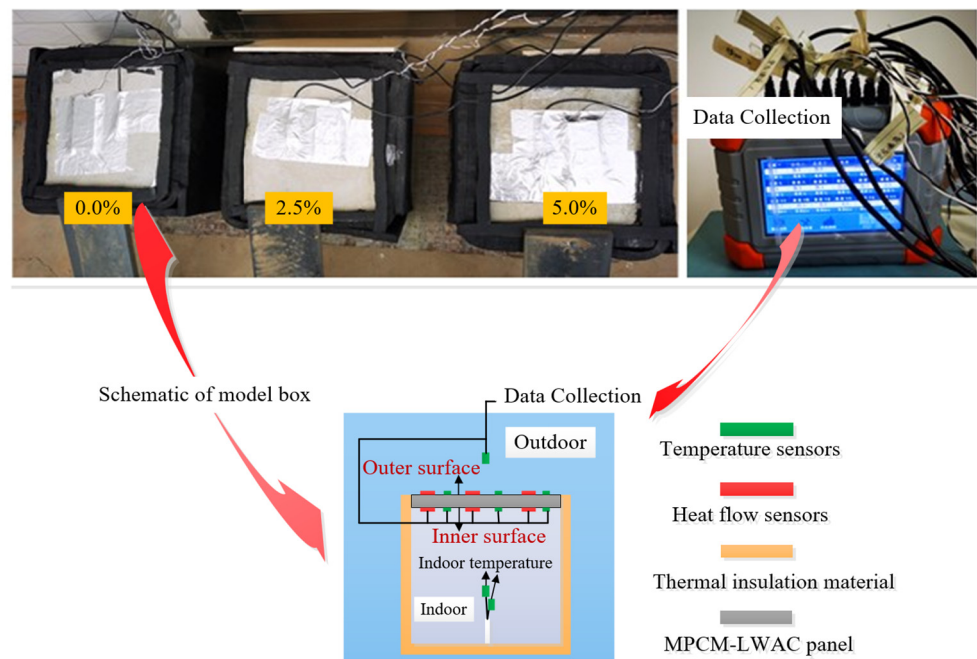


Figure 5. Model test.

3. Numerical Simulation

3.1. Heat Transfer Model

To investigate the effect of MPCM dosage, panel thickness, and outdoor temperature conditions on the thermal response of MPCM-LWAC panels, a numerical simulation was performed. In order to simplify the model, it is assumed that: (i) heat is transferred only along the panel's thickness direction; (ii) the MPCM-LWAC panel is homogeneous and isotropic; (iii) natural convection when the PCM is melted into a liquid is ignored; and (iv) there is no heat source inside the panel. Based on these assumptions, the equation for one-dimensional heat transfer across the MPCM-LWAC panel is shown in Equation (4).

$$k \frac{\partial^2 T}{\partial x^2} = \rho C_p(T) \frac{\partial T}{\partial t} \quad (4)$$

where “ k ”, “ ρ ”, and “ x ” are the thermal conductivity, dry density, and thickness of MPCM-LWAC, respectively, $W/(m \cdot ^\circ C)$, kg/m^3 , and mm ; “ $C_p(T)$ ” is the specific heat capacity as a function of the temperature of MPCM-LWAC, $J/(g \cdot ^\circ C)$.

3.2. Numerical Solution

The implicit difference method was applied to solve the mathematical model. As shown in Figure 6, the MPCM-LWAC panel was discretized into a number of nodes, where the distance (thickness) between two adjacent nodes is Δx .

Based on the energy balance equation and implicit difference method, the difference equation of each node inside the panel was obtained, as shown in Equation (5).

$$\begin{cases} k \frac{T_2^{t+\Delta t} - T_1^{t+\Delta t}}{\Delta x} + h_{in}(T_{in}^{t+\Delta t} - T_1^{t+\Delta t}) = \rho C_p \frac{\Delta x}{2} \frac{T_1^{t+\Delta t} - T_1^t}{\Delta t} & (i = 1) \\ k \frac{T_{m-1}^{t+\Delta t} - T_m^{t+\Delta t}}{\Delta x} + k \frac{T_{m+1}^{t+\Delta t} - T_m^{t+\Delta t}}{\Delta x} = \rho C_p \Delta x \frac{T_m^{t+\Delta t} - T_m^t}{\Delta t} & (2 \leq i \leq N - 1) \\ k \frac{T_{N-1}^{t+\Delta t} - T_N^{t+\Delta t}}{\Delta x} + h_{out}(T_{out}^{t+\Delta t} - T_N^{t+\Delta t}) = \rho C_p \frac{\Delta x}{2} \frac{T_N^{t+\Delta t} - T_N^t}{\Delta t} & (i = N) \end{cases} \quad (5)$$

where “ T_m^t ”, “ $T_m^{t+\Delta t}$ ” are the temperatures of node m at moments t and $(t + \Delta t)$, respectively, $^\circ C$; “ T_{in} ”, “ T_{out} ” are the internal and external ambient temperatures of the panel, respectively, $^\circ C$; “ h_{in} ”, “ h_{out} ” are the heat transfer coefficients of the inner and outer surfaces of the panel, respectively, $W/(m^2 \cdot K)$.

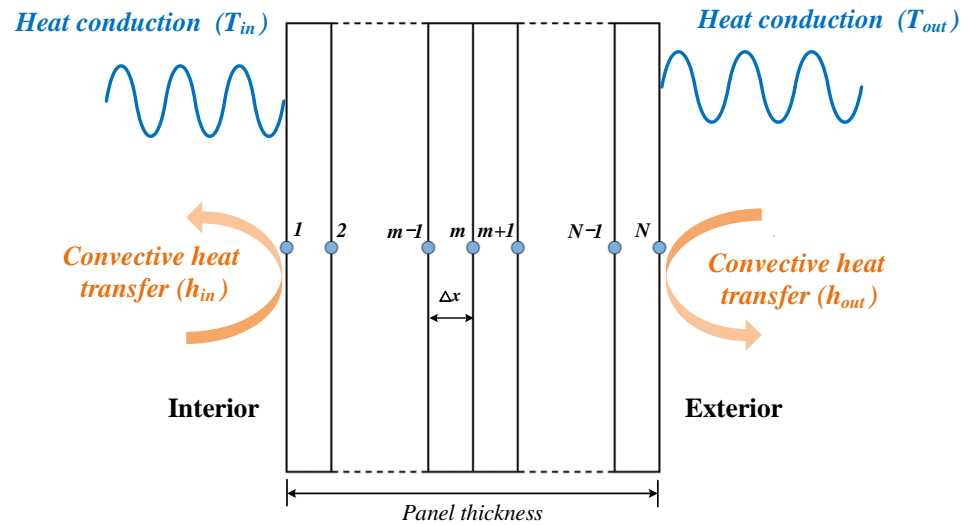


Figure 6. Discrete model and boundary conditions for the MPCM-LWAC panel.

3.3. Simulation Verification

Indoor and outer surface temperatures monitored in the model test (Section 2.4) were used as the temperature boundary conditions in the simulation study. The change of inner surface temperature (T_1) with time was obtained. The T_1 from the experiment and numerical simulation are presented in Figure 7. Figure 7 shows that the change trends of simulated data were basic coincidences with that of experimental data; however, a slight difference exists in the temperature. To evaluate the reliability of numerical solutions, the relative error (RAM) between the test results and simulation results was calculated using Equation (6). The calculation results showed that for panels with different MPCM dosages (0.0%, 2.5%, and 5.0%), the RAM is 2.0%, 2.1%, and 2.5% ($\leq 5\%$), respectively, indicating the reliability of the numerical results.

$$RAM = \text{Average} \left(\left| \frac{T_{1sim} - T_{1ref}}{T_{1ref}} \right| \times 100\% \right) \quad (6)$$

where " T_{1sim} " and " T_{1ref} " are the inner surface temperature of the MPCM-LWAC panel obtained by simulation and testing, respectively.

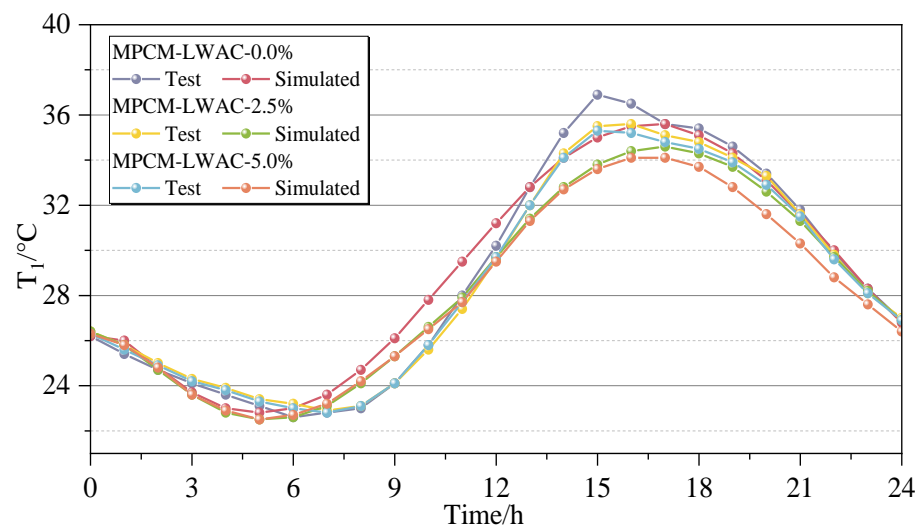


Figure 7. Inner surface temperature obtained from tests and simulations.

3.4. Simulated Working Conditions

According to the Thermal Design Code of Civil Building (GB50176-2016) [24], the convective heat transfer coefficients of the inner and outer surface of the panel can be set to $8.7 \text{ W}/(\text{m}^2 \cdot \text{K})$ and $19.0 \text{ W}/(\text{m}^2 \cdot \text{K})$, respectively. To research the effects of MPCM dosage, thickness, and outdoor temperature conditions on the thermal response of the MPCM-LWAC panel, the following three working conditions were designed to carry out numerical simulation studies. In addition, Equation (7) was used to simulate the outdoor temperature.

Case 1: Effect of MPCM dosage on thermal response.

Keeping the thickness of the panel at 35 mm, the dosages of MPCM in the MPCM-LWAC panel were 0.0%, 2.5%, 5.0%, 7.5%, and 10%, respectively.

Case 2: Effect of panel thickness on thermal response.

The MPCM content was taken as 0.0% and 5.0% (0.0% as a reference group), and the panel thicknesses were taken as 35 mm, 70 mm, 105 mm, and 140 mm.

For Case 1 and Case 2, A and B in Equation (7) were identified as $26 \text{ }^\circ\text{C}$ and $10 \text{ }^\circ\text{C}$, respectively.

Case 3: Effect of outdoor temperature conditions on thermal response.

Keeping the MPCM dosage (5.0%) and panel thickness (70 mm) unchanged, the different outdoor temperature conditions were simulated by changing the A and B in Equation (7). For Case 3, In order to simulate the thermal response of MPCM-LWAC panels exposed to various seasonal temperature conditions, A was set to vary from 0 to $40 \text{ }^\circ\text{C}$ in steps of $5 \text{ }^\circ\text{C}$. On the other hand, in order to investigate the effect of one-day temperature difference on the thermal response of MPCM-LWAC panels, B was set to different values, and this study took $4 \text{ }^\circ\text{C}$, $6 \text{ }^\circ\text{C}$, $8 \text{ }^\circ\text{C}$, and $10 \text{ }^\circ\text{C}$.

$$T_{out} = A + B \sin\left(\frac{\pi}{12}t\right) \quad (7)$$

where “A” represents the average outdoor temperature, $^\circ\text{C}$; “B” represents the outdoor temperature amplitude, $^\circ\text{C}$; “t” represents the time, h.

4. Results and Discussion

4.1. Analysis of Fundamental Properties

The fundamental properties (dry density, thermal conductivity, and specific heat capacity) of MPCM-LWAC with different MPCM dosages were tested and given in Figures 8 and 9.

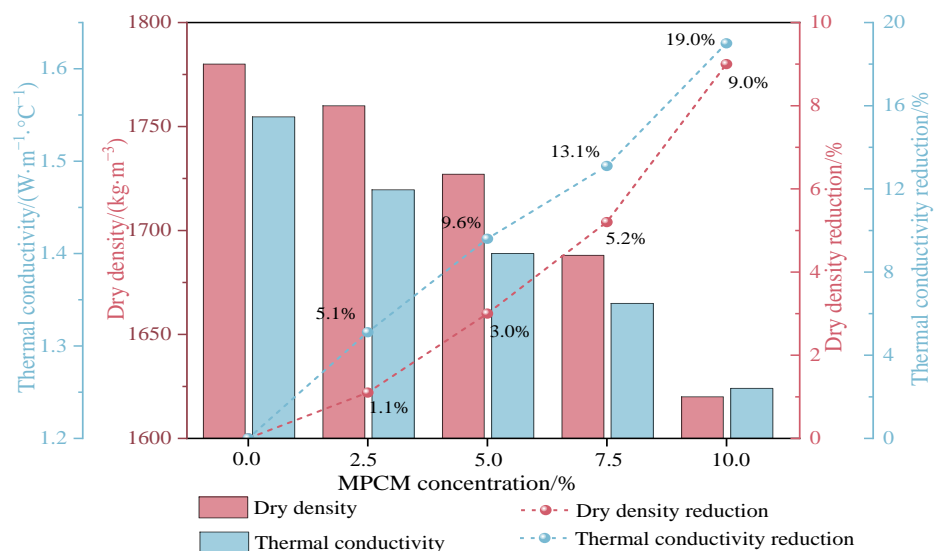


Figure 8. Effect of MPCM dosage on dry density and thermal conductivity of MPCM-LWAC.

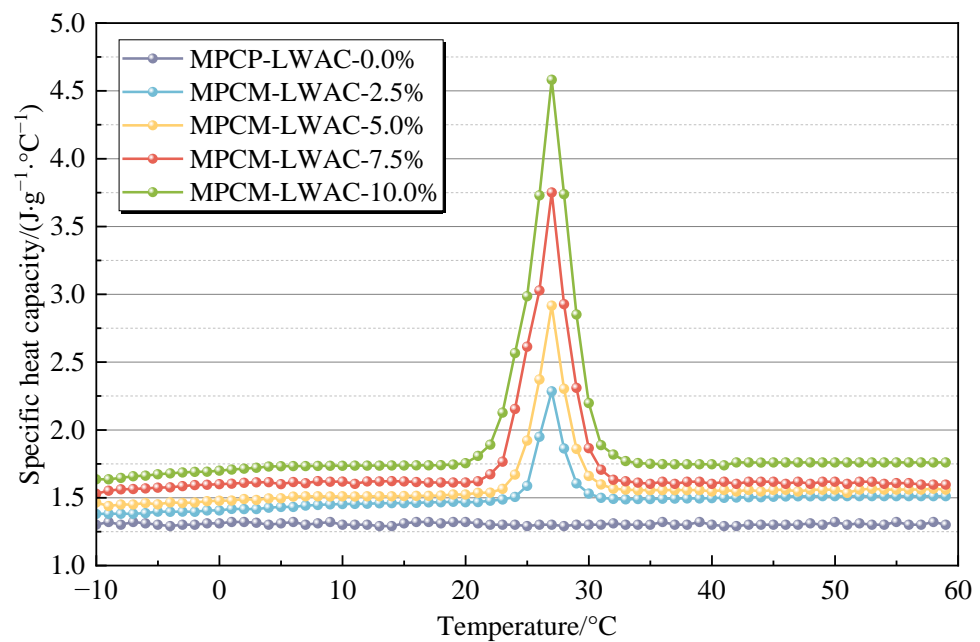


Figure 9. Effect of MPCM dosage on specific heat capacity of MPCM-LWAC.

Figure 8 shows that the dry density and thermal conductivity of MPCM-LWAC decreases as the MPCM dosage increases. When the dosage of MPCM increases from 0.0% to 10%, the dry density and thermal conductivity decrease by 9.0% and 19.0%, respectively. The reasons for this phenomenon may be that the density and thermal conductivity of MPCM are lower than those of the substituted shale ceramic sand. Moreover, the addition of MPCM leads to an increase in porosity, and air has a low density and low thermal conductivity ($0.0257 \text{ W}/(\text{m}\cdot^{\circ}\text{C})$) [25]. Figure 9 shows that in the tested temperature range, the temperature has almost no influence on the specific heat capacity of LWAC without MPCM. Within the range of phase transition temperature, the specific heat capacity of LWAC with MPCM varies considerably.

4.2. Analysis of Thermal Response

4.2.1. Effect of MPCM Dosage on Thermal Response

The effect of MPCM dosage on T_1 is shown in Figure 10a. According to Figure 10a, the temperature difference (ΔT_{dosage}) between the MPCM-LWAC panels with the MPCM dosage of 2.5%, 5.0%, 7.5%, and 10% and the MPCM-LWAC-0.0% panel were calculated, as shown in Figure 10b. Combining Figure 10a,b, it can be seen that with the increase in MPCM dosage, the peak temperature was delayed on one hand, and the fluctuation of T_1 was decreased on the other. This phenomenon is particularly noticeable in the melting (from 24.9°C to 28.9°C) and freezing (from 20°C to 25.1°C) temperature range of MPCM. Compared to the MPCM-LWAC-0.0% panel, the peak of T_1 for the MPCM-LWAC-10% panel is reduced by 0.4°C and its occurrence is delayed by 0.51 h.

Figure 11a shows the variation of heat flux of MPCM-LWAC panels when the MPCM dosage is 0.0%, 2.5%, 5.0%, 7.5%, and 10%. From Figure 11a, it can be seen that within the range of phase transition temperature, the more MPCM dosage, the smaller the change in the flux flow on the inner surface of the tested panel. Furthermore, the energy demand [26], an indicator assessing the energy-saving potential, can be obtained by calculating the cumulative heat flux through the inner surface of the tested panel. The results are given in Figure 11b. Figure 11b shows that when the MPCM dosage is 0.0%, 2.5%, 5.0%, 7.5%, and 10%, the energy demand of the MPCM-LWAC panel is $0.781 \text{ kWh}/\text{m}^2$, $0.759 \text{ kWh}/\text{m}^2$, $0.742 \text{ kWh}/\text{m}^2$, $0.717 \text{ kWh}/\text{m}^2$, and $0.687 \text{ kWh}/\text{m}^2$, respectively. That is to say, compared to the panel without MPCM, the energy demand of other panels with different MPCM dosages was reduced by 2.8%, 5.0%, 8.2%, and 12.0%, in turn.

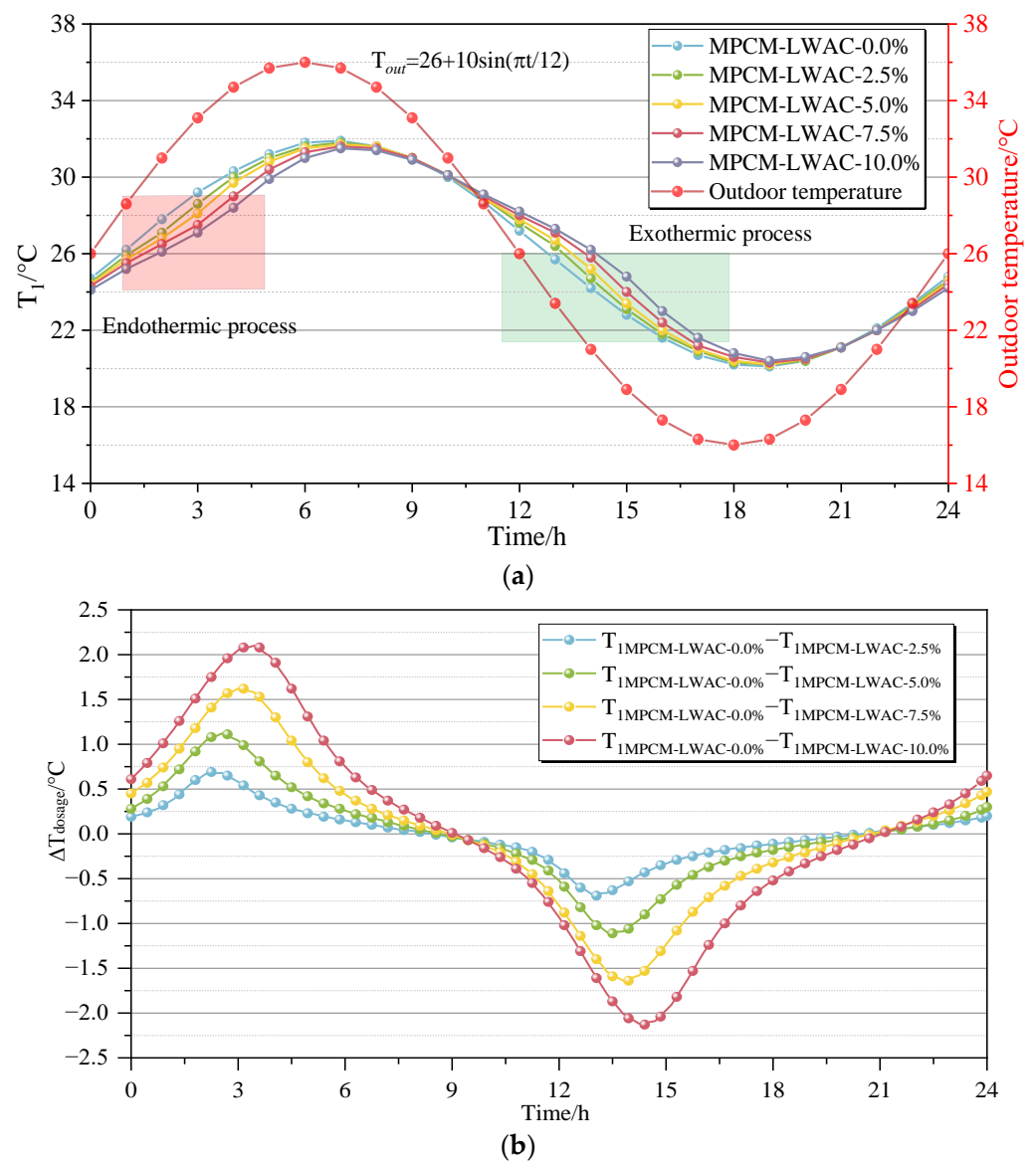


Figure 10. Effect of MPCM dosage on (a) inner surface temperature T_1 ; (b) temperature difference ΔT_{dosage} .

4.2.2. Effect of Panel Thickness on the Thermal Response

The panels with different thicknesses (Case 2 in Section 3.4) were simulated to investigate the effect of panel thickness on T_1 . The results are shown in Figure 12a. From Figure 12a, it can be seen that the fluctuation of T_1 in both the tested panels with and without MPCM decreases as the panel thickness increases. This is mainly due to the increase in thickness caused by the reduction of heat transfer in the unit area of the panel. For the MPCM-LWAC-0.0% panel and MPCM-LWAC-5.0% panel, when their thickness increased from 35 mm to 140 mm, the peak temperature (T_1) declined by 2.9 °C and 3.8 °C and was delayed by 3.21 h and 4.64 h, respectively. For the tested panel with the same thickness and different MPCM dosage, the temperature difference ($\Delta T_{thickness}$) was calculated according to Figure 12a, as shown in Figure 12b. A significant finding from Figure 12b was that when the panel thickness exceeded 105 mm, the increase in MPCM dosage did not cause the increase in $\Delta T_{thickness}$, but only delayed the time when the maximum value of $\Delta T_{thickness}$ appears.

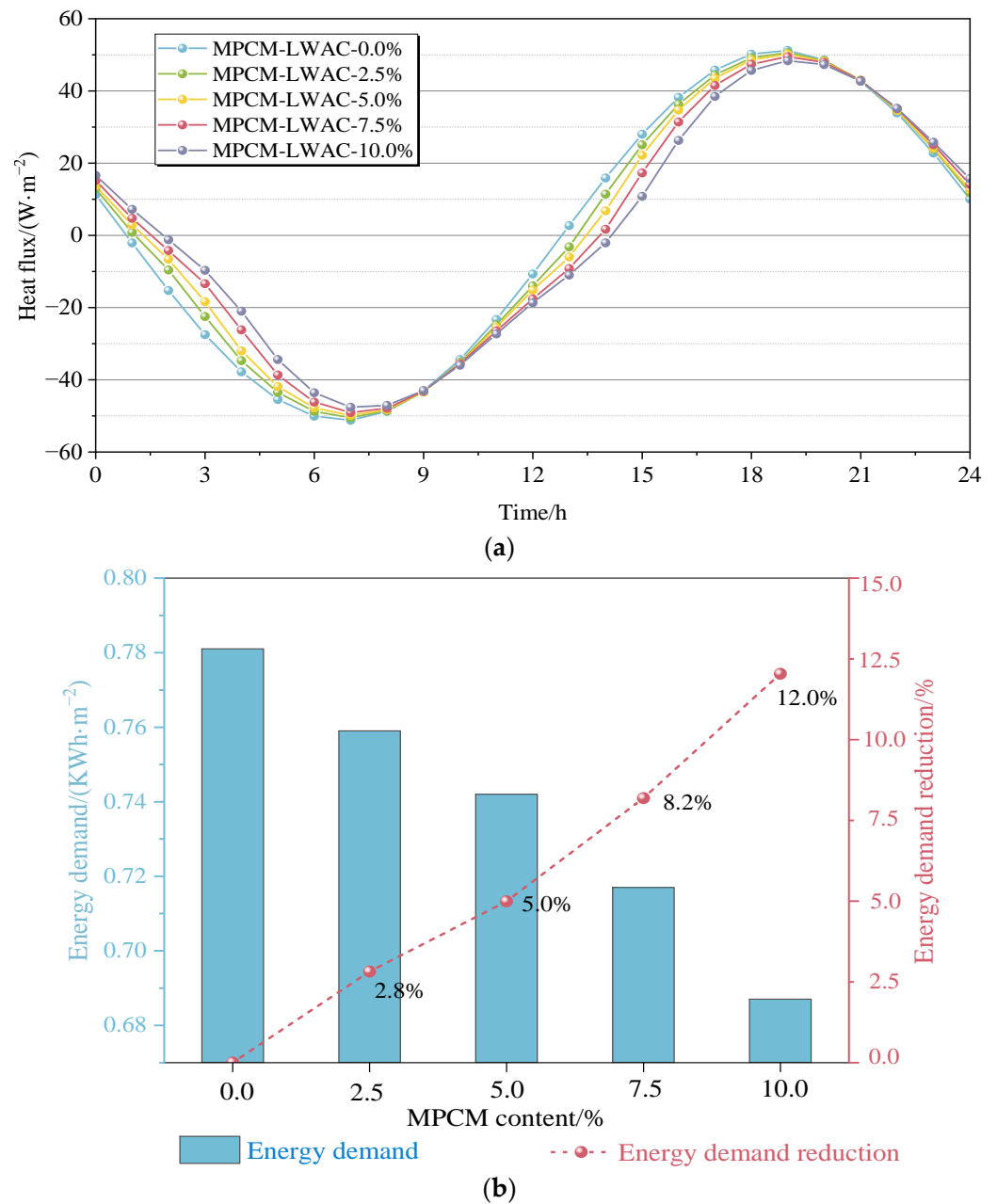


Figure 11. Effect of MPCM dosage on (a) heat flux; (b) energy demand.

For the MPCM-LWAC-0.0% panel and the MPCM-LWAC-5.0% panel with different thicknesses, the heat flux and energy demand were given in Figure 13a,b. Figure 13b shows that when the panel thickness increases from 35 mm to 140 mm, the energy demand decreases from $0.781 \text{ KWh}/\text{m}^2$ to $0.394 \text{ KWh}/\text{m}^2$ for the MPCM-LWAC-0.0% panel, and decreases from $0.742 \text{ KWh}/\text{m}^2$ to $0.255 \text{ KWh}/\text{m}^2$ for the MPCM-LWAC-5.0% panel. For an increase in MPCM-LWAC-5.0% panel thickness from 35mm to 70mm, 105mm, and 140mm, the energy demand is reduced by 25.7%, 48.7%, and 65.6%, respectively.

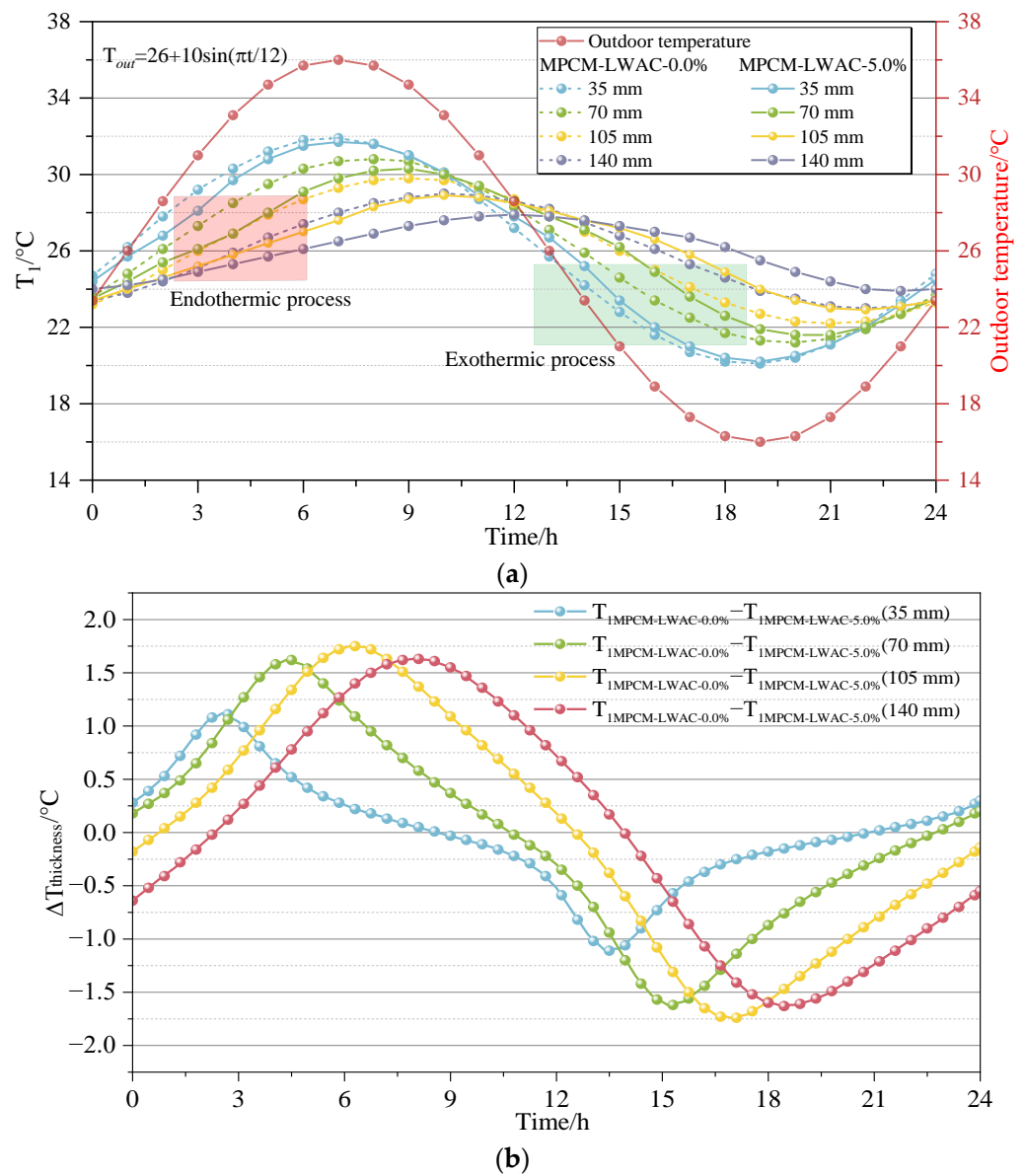


Figure 12. Effect of thickness on (a) inner surface temperature T_1 ; (b) temperature difference $\Delta T_{thickness}$.

4.2.3. Effect of Outdoor Temperature Conditions on the Thermal Response

The effect of outdoor temperature conditions on T_1 of the tested panel was studied. Three groups of outdoor temperature conditions were selected and given in Figure 14a. Figure 14b gives the temperature difference ($\Delta T_{outdoor}$) of T_1 of tested panels under different outdoor temperature conditions. Figure 14a,b shows clearly that when the average outdoor temperature is 0 °C, 25 °C, and 40 °C, the $\Delta T_{outdoor}$ (the tested panel without MPCM and with 5.0% MPCM) are $-0.6 \sim 0$ °C, $-1.4 \sim 1.3$ °C, and $-0.3 \sim 0.6$ °C, respectively. This finding helps to determine the optimal outdoor temperature conditions for the application of the MPCM-LWAC panel.

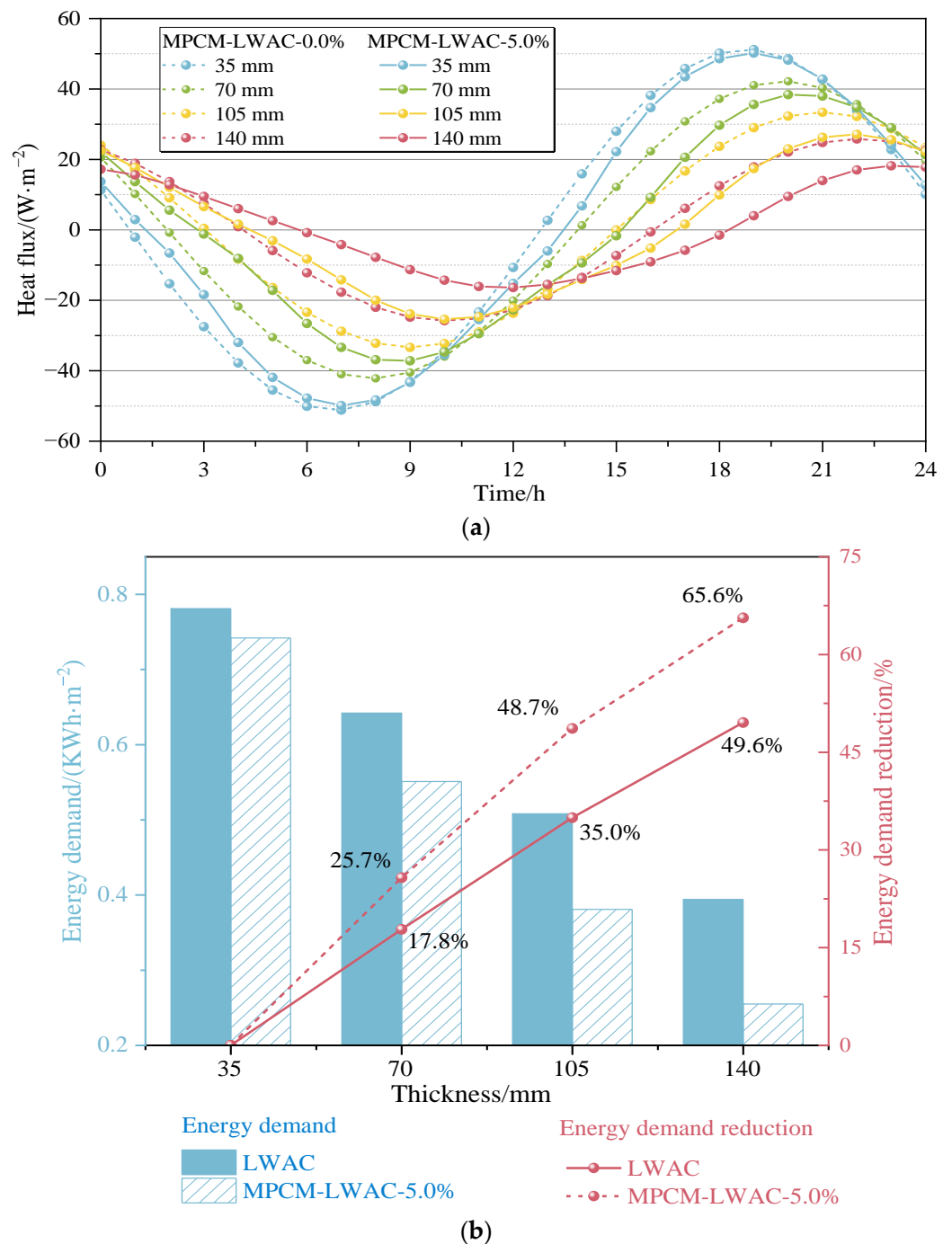


Figure 13. Effect of thickness on (a) heat flux; (b) energy demand.

Similarly, the energy demand of the tested panels under various outdoor temperature conditions was calculated, and the results were given in Figure 15a. Figure 15a shows that for the MPCM-LWAC-0.0% panel and the MPCM-LWAC-5.0% panel, with the increasing of outdoor average temperature, the energy demand first decreases, reaches its minimum at an average outdoor temperature of 25 °C, and then increases. That is to say, the energy demand is much lower when the average outdoor temperature is close to the melting temperature of MPCM and the outdoor temperature fluctuation is low throughout the day. According to Figure 15a, the reduction in energy demand of the tested panels was calculated and shown in Figure 15b. As can be seen from Figure 15b, the energy demand reduction of the MPCM-LWAC-5.0% panel achieves the maximum (about 15~17%) at the average outdoor temperature of 25 °C. For the higher (>30 °C) and lower (<20 °C) outdoor

average temperatures, the addition of MPCM has a smaller impact on reducing energy demand. The reason for this phenomenon was closely related to the phase-transition temperature range of MPCM. In addition, Figure 15b also shows that energy demand was reduced by about 2% at the higher and lower outdoor average temperatures, which may be caused by the decrease in thermal conductivity of LWAC incorporated with MPCM.

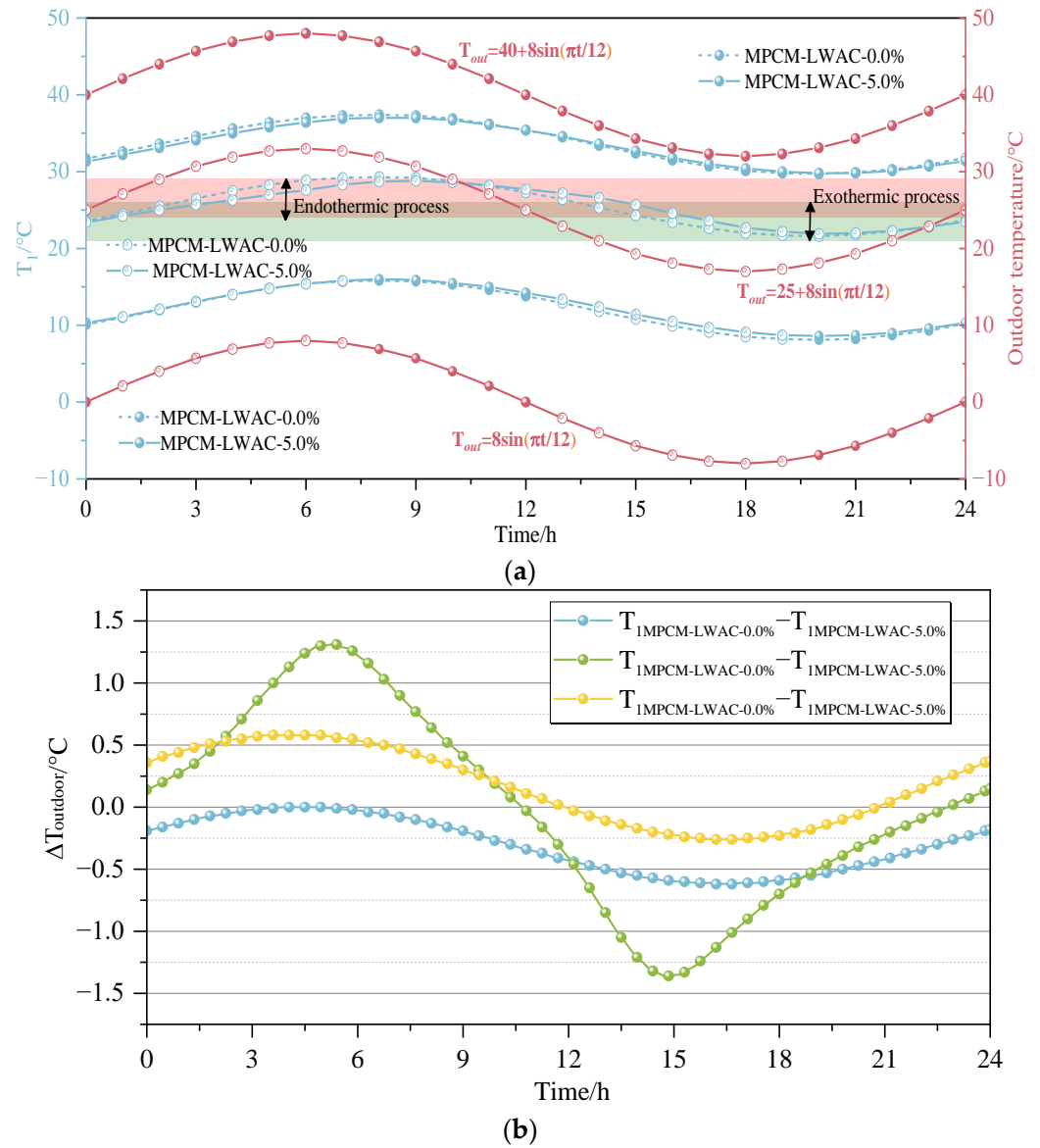


Figure 14. Effect of outdoor temperature conditions on (a) inner surface temperature T_1 ; (b) temperature difference $\Delta T_{outdoor}$.

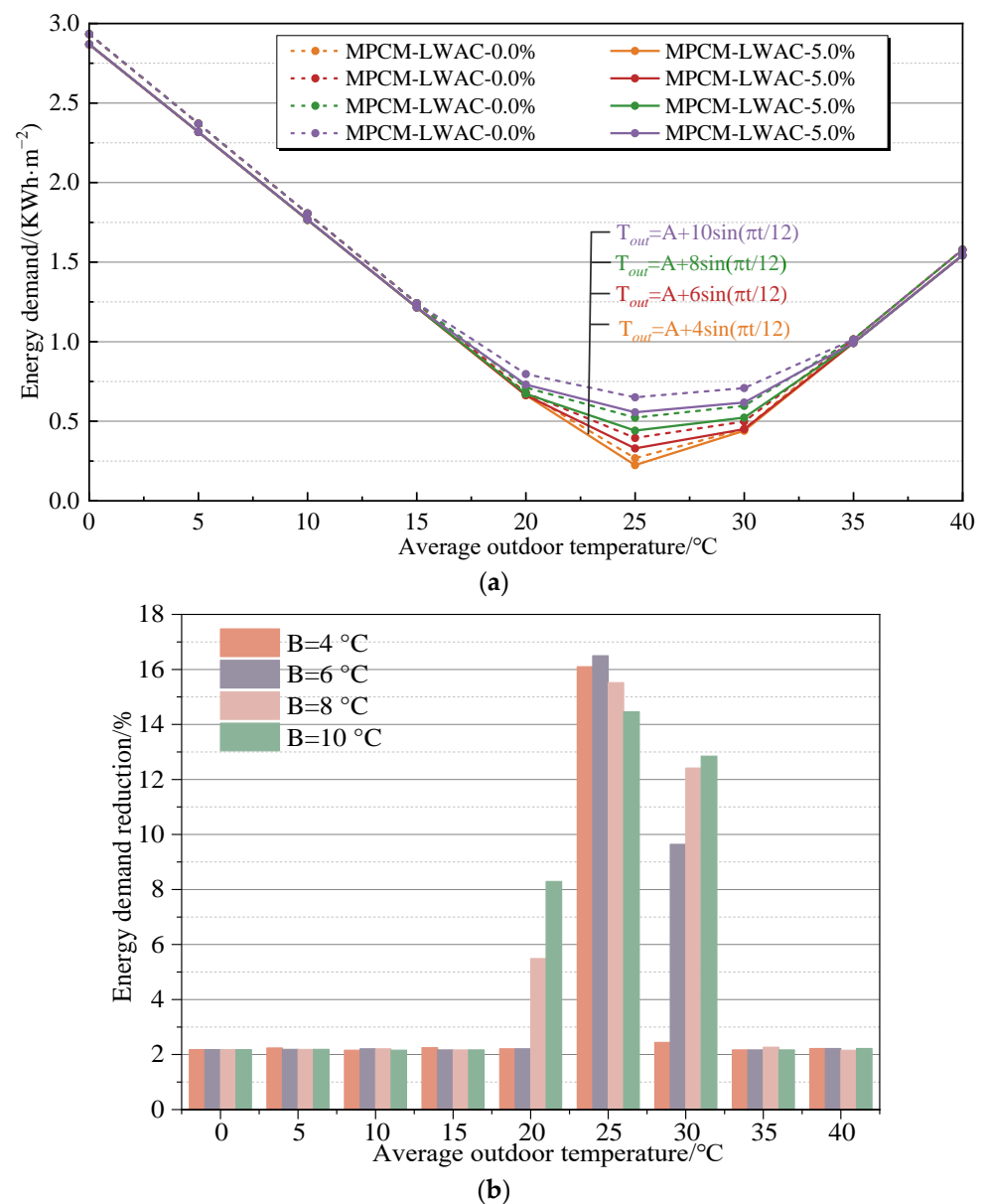


Figure 15. Effect of outdoor temperature conditions on (a) energy demand; (b) energy demand reduction.

5. Conclusions

With the objective of surveying the optimum design parameters and the best working conditions of the MPCM-LWAC panel, experimental and numerical research was carried out to determine the effect of MPCM dosage, panel thickness, and outdoor temperature conditions on the thermal response of the tested panels. The main findings of this research are as follows.

(1) With the increasing of MPCM dosage, dry density and thermal conductivity of MPCM-LWAC panels decrease but specific heat capacity increases. Comparing MPCM-LWAC-10.0% with MPCM-LWAC-0.0%, its dry density and thermal conductivity decrease by 9.0% and 19.0%, respectively.

(2) In terms of the effect of MPCM dosage on thermal response, the addition of MPCM contributes to the reduction and delay of the inner surface temperature of the MPCM-LWAC panel, and such reduction and delay are proportional to the MPCM dosage. For the MPCM-LWAC panel with a thickness of 35 mm, when the dosage of MPCM is increased from

0% to 10%, the lower energy demand maintaining the comfortable interior temperature is reduced by 12.0%.

(3) In terms of the effect of panel thickness on thermal response, the optimal value of the thickness of the MPCM-LWAC panel is 105 mm. For the MPCM-LWAC-5.0% panel, when panel thickness is greater than 105 mm, the addition of MPCM only delays the peak temperature. In addition, when the thickness increases from 35 mm to 140 mm, the energy demand is reduced by 65.6%.

(4) The best use condition of the MPCM-LWAC panel is obtained by quantitative analysis of the effect of outdoor temperature conditions on its thermal response. With the increasing average outdoor temperature, energy demand decreases at first and then increases. When the average outdoor temperature is 25 °C, energy demand reaches the minimum (0.224 kWh/m²).

(5) This study determines the best design parameters and use conditions of the MPCM-LWAC panel, providing a basis for the application of MPCM-LWAC in building envelope structures.

Author Contributions: Conceptualization, L.Z. and G.S.; methodology, L.Z. and Q.W.; data curation, Q.W.; writing—original draft preparation, Q.W.; writing—review and editing, Z.C. and Y.X. funding acquisition, L.Z. and G.S. All authors have read and agreed to the published version of the manuscript.

Funding: This research is sponsored by the National Natural Science Foundation of China (no. 52078420, 52208289), Shaanxi Provincial Key Research and Development Project (no. 2020ZDLNY06-05), and Young Talent Fund of Association for Science and Technology in Shaanxi, China (no. 20230464).

Data Availability Statement: The data used to support the findings of this study are included within the article.

Conflicts of Interest: The authors declare no conflicts of interest.

References

1. Wang, R.; Ren, M.; Gao, X.J.; Qin, L. Preparation and properties of fatty acids based thermal energy storage aggregate concrete. *Constr. Build. Mater.* **2018**, *165*, 1–10. [[CrossRef](#)]
2. Shi, J.Y.; Tan, J.X.; Liu, B.J.; Liu, Y.C.; Xu, H.J.; Wang, Z.H.; Xiong, T.Y. Thermal and mechanical properties of thermal energy storage lightweight aggregate mortar incorporated with phase change material. *J. Energy Storage* **2020**, *32*, 101719. [[CrossRef](#)]
3. Liu, J.; Xue, Y.; Fu, Y.; Yao, K.; Liu, J.Q. Numerical investigation on microwave-thermal recovery of shale gas based on a fully coupled electromagnetic, heat transfer, and multiphase flow model. *Energy* **2023**, *263*, 126090. [[CrossRef](#)]
4. Tian, G.H.; Lv, H.L.; Huang, J.E.; Liu, P.; Feng, W. Experimental study on the thermal performance of a wall coated with a phase-change, energy-storing mortar layer during summer. *Appl. Therm. Eng.* **2017**, *124*, 279–285. [[CrossRef](#)]
5. Wang, L.C.; Xue, Y.; Cao, Z.Z.; Kong, H.L.; Han, J.Y.; Zhang, Z.Z. Experimental study on mode I fracture characteristics of granite after low temperature cooling with liquid nitrogen. *Water* **2023**, *15*, 3442. [[CrossRef](#)]
6. Akeiber, H.; Nejat, P.; Majid, M.Z.A.; Wahid, M.A.; Jomehzadeh, F.; Famileh, I.Z.; Calautit, J.K. A review on phase change material (PCM) for sustainable passive cooling in building envelopes. *Renew. Sustain. Energy Rev.* **2016**, *60*, 1470–1497. [[CrossRef](#)]
7. Marin, P.; Saffari, M.; Gracia, A.D.; Zhu, X.B.Y.; Farid, M.M.; Cabeza, L.F.; Ushak, S. Energy savings due to the use of PCM for relocatable lightweight buildings passive heating and cooling in different weather conditions. *Energy Build.* **2016**, *129*, 274–283. [[CrossRef](#)]
8. Berardi, U.; Gallardo, A.A. Properties of concretes enhanced with phase change materials for building applications. *Energy Build.* **2019**, *199*, 402–414. [[CrossRef](#)]
9. Mustafa, J.; Alqaed, S.; Sharifpur, M. Loading phase change material in a concrete based wall to enhance concrete thermal properties. *J. Build. Eng.* **2022**, *56*, 104765. [[CrossRef](#)]
10. Li, W.; Zhang, Y.L.; Zhang, X.; Zhao, J. Studies on performance enhancement of heat storage system with multiple phase change materials. *J. Energy Storage* **2022**, *47*, 103585. [[CrossRef](#)]
11. Cunha, S.; Leite, P.; Aguiar, J. Characterization of innovative mortars with direct incorporation of phase change materials. *J. Energy Storage* **2020**, *30*, 101439. [[CrossRef](#)]
12. Cunha, S.; Silva, M.; Aguiar, J. Behavior of cementitious mortars with direct incorporation of non-encapsulated phase change material after severe temperature exposure. *Constr. Build. Mater.* **2020**, *230*, 117011. [[CrossRef](#)]
13. Ren, M.; Liu, Y.S.; Gao, X.J. Incorporation of phase change material and carbon nanofibers into lightweight aggregate concrete for thermal energy regulation in buildings. *Energy* **2020**, *197*, 117262. [[CrossRef](#)]

14. Wu, T.J. Study on the preparation and properties of paraffin phase change energy storage of the concrete. *New Build. Mater.* **2016**, *43*, 91–93.
15. Mokhtari, S.; Madhkan, M. The performance effect of PEG-silica fume as shape-stabilized phase change materials on mechanical and thermal properties of lightweight concrete panels. *Case Stud. Constr. Mater.* **2022**, *17*, e01298. [[CrossRef](#)]
16. Ma, Q.Y.; Bai, M. Preparation and properties of phase-change energy-storage concrete. *Acta Mater. Compos. Sin.* **2018**, *35*, 676–683.
17. Zhu, J.Q.; Li, J.L.; Zhou, W.B.; Li, R.G. Preparation and characterization of a capric acid-stearic acid-ceramsite-concrete composite phase change material. *Energy Storage Sci. Technol.* **2017**, *6*, 255–262.
18. Memon, S.A.; Cui, H.Z.; Zhang, H.; Xing, F. Utilization of macro encapsulated phase change materials for the development of thermal energy storage and structural lightweight aggregate concrete. *Appl. Energy* **2015**, *139*, 43–55. [[CrossRef](#)]
19. Li, M.; Zhou, D.Y.; Jiang, Y.Q. Preparation and thermal storage performance of phase change ceramsite sand and thermal storage light-weight concrete. *Renew. Energy* **2021**, *175*, 143–152. [[CrossRef](#)]
20. Urgessa, G.; Yun, K.K.; Yeon, J.; Yeon, J.H. Thermal responses of concrete slabs containing microencapsulated low-transition temperature phase change materials exposed to realistic climate conditions. *Cem. Concr. Compos.* **2019**, *104*, 103391. [[CrossRef](#)]
21. Yin, G.S.; Zhang, J.T.; Shi, M.H.; Chen, W.B.; Zheng, X.H.; Wei, P.F.; Feng, J.J. Thermal properties of phase change thermal storage foam concrete. *Acta Mater. Compos. Sin.* **2023**, *40*, 4246–4259.
22. Sukontasukkul, P.; Sangpe, T.; Newlands, M.; Yoo, D.Y.; Tangchirapat, W.; Limkatanyu, S.; Chindaprasirt, P. Thermal storage properties of lightweight concrete incorporating phase change materials with different fusion points in hybrid form for high temperature applications. *Heliyon* **2020**, *6*, e04863. [[CrossRef](#)] [[PubMed](#)]
23. Zhu, L.; Dang, F.N.; Xue, Y.; Jiao, K.; Ding, W.H. Multivariate analysis of effects of microencapsulated phase change materials on mechanical behaviors in light-weight aggregate concrete. *J. Build. Eng.* **2021**, *42*, 102783. [[CrossRef](#)]
24. GB50176-2016; Thermal Design Code for Civil Building. China Architecture & Building Press: Beijing, China, 2017.
25. Zhu, L.; Ding, W.H.; Dang, F.N.; Sang, G.C.; Xue, Y.; Wang, Q.Y. Combined experimental and theoretical investigation of pore characteristics effect on thermal conductivity of light-weight aggregate concrete including microencapsulated PCM. *J. Mater. Res. Technol.* **2023**, *26*, 587–602. [[CrossRef](#)]
26. Ye, R.D.; Huang, R.; Fang, X.M.; Zhang, Z.G. Simulative optimization on energy saving performance of phase change panels with different phase transition temperatures. *Sustain. Cities Soc.* **2020**, *52*, 101833. [[CrossRef](#)]

Disclaimer/Publisher’s Note: The statements, opinions and data contained in all publications are solely those of the individual author(s) and contributor(s) and not of MDPI and/or the editor(s). MDPI and/or the editor(s) disclaim responsibility for any injury to people or property resulting from any ideas, methods, instructions or products referred to in the content.